

# Control-Oriented Compressor Model with Adiabatic Efficiency Extrapolation

Xavier Llamas and Lars Eriksson  
Vehicular Systems, Linköping University

## ABSTRACT

Downsizing and turbocharging with single or multiple stages has been one of the main solutions to decrease fuel consumption and harmful exhaust emissions, while keeping a sufficient power output. An accurate and reliable control-oriented compressor model can be very helpful during the development phase, as well as for engine calibration, control design, diagnostic purposes or observer design. A complete compressor model consisting of mass flow and efficiency models is developed and motivated. The proposed model is not only able to represent accurately the normal region measured in a compressor map but also it is capable to extrapolate to low compressor speeds. Moreover, the efficiency extrapolation is studied by analyzing the known problem with heat transfer from the hot turbine side, which introduces errors in the measurements done in standard gas stands. Since the parameterization of the model is an important and necessary step in the modeling, a tailored parameterization approach is presented based on Total Least Squares. A standard compressor map is the only data required to parameterize the model. The parameterization is tested with a database of more than 230 compressor maps showing that it can deal well with different compressor sizes and characteristics. Also, general initialization values for the model parameters are provided using the complete database parameterization results. The results show that the model accuracy is good and in general achieves relative errors below one percent. A comparison of the model accuracy for compressor maps with and without heat transfer influence is carried out, showing a similar model accuracy for both cases but better when no heat transfer is present. Furthermore, it is shown that the model is capable to predict the efficiency characteristics at low speed of two compressor maps, measured with near adiabatic conditions.

## 1 INTRODUCTION

The legislation pressure on the exhaust emission limits drive the automotive industry into researching more advanced technologies. Moreover, the increasing fuel prices, also push the need to develop more and more fuel efficient internal combustion engines (ICE). One of the most popular solutions to achieve these

demands is downsizing and turbocharging the ICE. Many examples of boosting systems exist nowadays, e.g. from various turbocharger stages to electrically driven compressors. Introducing more and newer components into a ICE makes the complete system more complex to deal with. First, in terms of system design choices, later due to the complexity that arises from having to control the ICE as efficient as possible. In order to overcome this, having a simulation model to apply model-based control techniques can be very useful to benchmark different system architectures as well as to test different control strategies.

In model-based control, a model that is capable to capture the main dynamic characteristics of the system is required. At the same time, this model has to be computationally low demanding. Mean value engine models (MVEM) fulfill these two requirements, and have been successfully applied to many different types of combustion engines, see e.g. [1, 2, 3]. A control-oriented compressor model is required as a part of the complete MVEM. This family of compressor models has also received significant attention in the automotive research literature, see among many others [4, 5, 6, 7, 8, 9].

In the research literature, the compressor efficiency modeling has received less attention than the mass flow modeling. One reason for that could be the known problem with heat transfer from the hot turbine gases in the gas stand, which introduces errors in the compressor efficiency measurements. This issue has a greater effect at low compressor speeds, as it is pointed out in [10, 11, 12, 13, 14] among many others. The fact that normal compressor maps are only measured down to 35% – 40% of the maximum rotational speed adds even more uncertainty to what is the true value of the compressor efficiency in this area. This in turn makes the validation of the efficiency extrapolation a difficult task.

The main objective of this investigation is to continue the work carried out in [15] for centrifugal compressors used in marine propulsion. The focus here is to apply the modeling approach together with an updated estimation procedure to automotive compressors. Hence, the general applicability of the model and parameterization method to any compressor size is demonstrated. At the same time an investigation of how the heat transfer affects the compressor efficiency is done. This motivates some changes in the efficiency model compared to

the one proposed in [15], in order to be able to describe as good as possible the adiabatic efficiency at low compressor speeds.

## 2 COMPRESSOR PERFORMANCE

The performance of a centrifugal compressor is characterized by its compressor map. The map contains measurements of several different operating points at different compressor speeds. Measurements with the same compressor speed are connected together in the compressor map forming a Speed Line (SpL). The usual map variables are pressure ratio  $\Pi_c = \frac{p_{02}}{p_{01}}$ , efficiency  $\eta_c$ , corrected speed  $\bar{N}_c$  and corrected mass flow  $\bar{W}_c$ . The corrected variables are computed as in [16]

$$\bar{N}_c = N_c \frac{1}{\sqrt{T_{01}/T_{c,ref}}} \quad (1)$$

$$\bar{W}_c = W_c \frac{\sqrt{T_{01}/T_{c,ref}}}{p_{01}/p_{c,ref}} \quad (2)$$

where  $T_{c,ref}$  and  $p_{c,ref}$  are the reference values. A complete nomenclature list can be found at the appendix. The derivation of the correction formulas is done using dimensional analysis, a complete explanation can be found in [17, 18, 19]. The main reason to have corrected quantities in the compressor map is to cover different inlet conditions with a single compressor map. Thus, for the corrected quantities to fulfill its purpose, the same pair of values ( $\bar{N}_c$ ,  $\bar{W}_c$ ) achieved with different inlet conditions should give the same pressure ratio and efficiency values. However, deviations of pressure ratio for the same corrected variables but with different pressure inlet conditions are observed in [20]. A similar study but for the efficiency case would be very interesting, but it is out of the scope of this study.

### Compressor Efficiency and Heat Transfer

In a combustion engine installation, compressor operation will not be adiabatic. Nevertheless, knowing the true adiabatic performance of the compressor is important, since the heat transfer characteristics of the gas stand are not the same as in the combustion engine. This mismatch will introduce errors as pointed out in [12]. In case an accurate compressor outlet temperature is desired, the model can be complemented with a heat transfer model of the turbocharger, see e.g. [12, 21].

Compressor efficiency measures of how much of the mechanical energy available in the compressor shaft is used to increase the pressure of the working fluid. There are many definitions of compressor efficiency, see e.g. [18]. Through this study the isentropic definition is going to be used. When measuring a compressor performance map, efficiency is usually calculated from the total pressures and temperatures at the inlet,  $(T_{01}, p_{01})$ , and at the outlet,  $(T_{02}, p_{02})$ . Total pressures are computed as the sum of the static value plus a term corresponding to the velocity of the fluid, see 17 for more information. Using the total to total

isentropic definition, the efficiency is computed as

$$\eta_c = \frac{\Delta h_{is}}{\Delta h_{act}} = \frac{\frac{p_{02}}{p_{01}}^{\frac{\gamma-1}{\gamma}} - 1}{\frac{T_{02}}{T_{01}} - 1} \quad (3)$$

where  $\Delta h_{is}$  represents the required power to compress the fluid in the ideal case that the compression is done isentropically. On the other hand,  $\Delta h_{act}$ , represents the actual power required to compress the fluid. More information about this efficiency definition and its derivation can be found in [18, 19].

From this expression it is easy to identify that errors in the measured pressure ratio will affect the efficiency, see [22]. However, the inlet and outlet temperatures are the most critical measurements for the efficiency accuracy. If the temperature measurement is influenced by external heat transfer from the hot turbine side, the measurement and the calculated efficiency will be inaccurate. Furthermore, temperature measurements are always difficult to carry out. Heat transfer effects on efficiency measurements have received much attention in literature, see e.g. [10, 12, 13, 14, 21, 23, 24, 25, 26]. In particular, as pointed out in [10] and [23], the effects of the heat transfer in the efficiency measurements have a greater influence at low compressor speeds and low flows. Coolant water and lubricating oil temperature and pressure will affect the measured efficiency as well, see [10, 14]. On the other hand, heat transfer practically does not affect the mass flow and pressure ratio measurements as it can be seen in [10].

A method to assess whether or not the measured efficiency is affected by heat transfer is to plot the Euler work input coefficient  $\lambda_{Euler}$ , as function of the flow coefficient at the impeller outlet  $\phi_2$ . These two variables should follow a linear dependence, see [27], following a mathematical function of the form

$$\lambda_{Euler} = 1 - \frac{c_s}{U_2} + \phi_2 \tan \beta_2 \quad (4)$$

where  $c_s/U_2$  represents the slip factor and  $\tan \beta_2$  is negative for a backswept impeller. The impeller outlet flow coefficient is not straightforward to compute with the usual signals available in a compressor map, thus it is better to rewrite (4) for the inlet flow coefficient as it is done in [27]. This can be done with the help of the change of density of the working fluid during the impeller stage, which yields to the following equation

$$\lambda_{Euler} = 1 - \frac{c_s}{U_2} + \phi_1 \frac{D_2}{b_2 \pi} \frac{\tan \beta_2}{[1 + (\gamma - 1)\gamma_{imp}\lambda M_{U_2}^2]^{n_{imp}-1}} \quad (5)$$

where  $\lambda$  is the work input coefficient,  $\gamma_{imp}$  is the kinematic degree of reaction,  $M_{U_2}$  is the tip-speed Mach number and  $n_{imp}$  is the polytropic exponent. The disc friction losses on the impeller disc establish the relation between the work input coefficient  $\lambda$ , and the euler work input coefficient  $\lambda_{Euler}$ , which can be expressed as

$$\lambda = \left(1 + \frac{k_{fric}}{\phi_1}\right) \lambda_{Euler} \quad (6)$$

According to [23, 24], the different speed lines of the compressor should collapse into a single line in the  $\lambda_{Euler} - \phi_2$

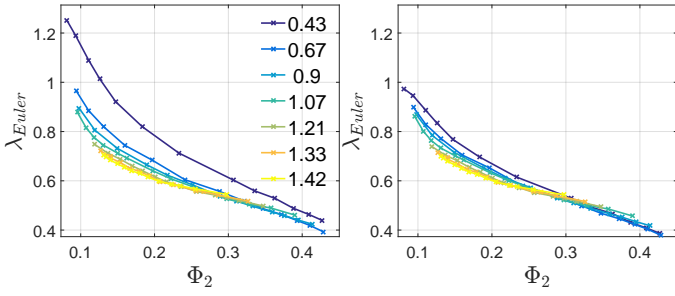


Figure 1: Euler work input coefficient vs outlet flow coefficient. Left; no heat transfer correction. Right; with the correction applied. The values in the legend correspond to different tip speed Mach numbers.

plane, unless there is heat transfer affecting the efficiency measurements. Note that in order to compute  $\phi_2$ , compressor geometry details are required to calculate the velocity triangle at the impeller outlet. Since this information is not usually available in the usual compressor maps, the iterative method presented in [27] can be used to obtain  $\phi_2$  for vaneless diffuser compressors. For vaned diffuser compressors, a similar method but with different assumptions could be derived. The only geometrical parameters required are the impeller outlet wheel diameter,  $D_2$ , and the not always available diffuser width,  $b_2$ . Based on empirical measurements of compressor impellers and data available in the database, a value between 7 – 10% of the diameter  $D_2$  is a fair approximation of  $b_2$ . With  $\phi_2$  available, the correction method based on constant heat transfer from the hot turbine side, described in [23], can be applied. It requires a single parameter for the complete map correction that needs to be properly calculated.

An example of a corrected Euler work input coefficient vs outlet flow coefficient can be seen in Figure 1. The Figure contains the same plot with and without applying the heat correction method. It clearly shows the lowest speed line having a much larger working input coefficient than the rest in the uncorrected measurements. When the Euler work input coefficient is corrected for adiabatic conditions, the efficiency lines are moved towards higher efficiency values.

It is important to mention that the obtained efficiency after the correction cannot be considered the exact adiabatic efficiency, since the correction method introduces uncertainties and assumptions. Moreover, the usual compressor maps do not contain much information about how the measurements are made. For example knowing if the turbine inlet temperature has been the same for all measured SpLs is important to be able to apply the correction method successfully.

### 3 EXPERIMENTAL DATA

A database of compressor maps is used to develop and validate the compressor model. The database contains 234 automotive compressor maps of different sizes from several manufacturers. The main characteristics of the database are depicted in Figure

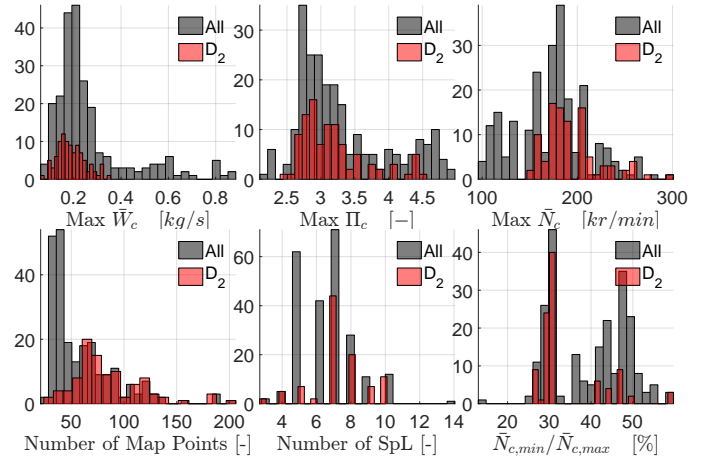


Figure 2: Histogram of the main characteristics of the compressor map database in gray. In red the main characteristics of the compressors with available outer impeller diameter,  $D_2$ .

2. A subset of 98 compressor maps with available outer impeller diameter  $D_2$  is selected from the database. This is done in order to be able to apply the heat correction method discussed in Section 2 and originally developed in [23]. An overview of the main characteristics of these maps is presented in Figure 2. It is interesting to note, as it can be seen in Figure 2, that there are very few maps with measured compressor speeds below 30% of the maximum compressor speed.

Two extended compressor maps, which are not included in the 234 database maps, are used to validate the extrapolation of the model at low compressor speeds. These maps, named TD04 and K04, are measured respectively down to 12% and 13% of the maximum measured speed. Furthermore, in order minimize the heat transfer effects on the measured efficiency, the turbine inlet temperature in the gas stand is kept at 300K for the lower speed lines. Also the oil temperature and the coolant water temperature are kept as close as possible to the compressor outlet temperature. These conditions are considered to be really close to the true adiabatic case, see [10], thus these maps are called near adiabatic maps.

### 4 COMPRESSOR MODEL

The main purpose of the compressor modeling is to describe the compressor performance as a set of mathematical functions. The complete compressor model consists of a submodel to compute the compressor mass flow, and another submodel to compute the compressor efficiency. In a MVEM simulation, the surrounding pressures and the turbocharger speed are normally state variables. Hence, the compressor model is called with the following input-output relation

$$[W_c, \eta_c] = \text{CompressorModel}(\Pi_c, N_c) \quad (7)$$

with this setup, is important to note that efficiency and mass flow will be signals computed with the model, consequently its

accuracy will be dependent on the modeling errors.

The model base functions are normalized, this is done in order to have similar parameter values regardless of the compressor physical size. First of all, this becomes very useful for the initialization of the model parameters for any given compressor map. Furthermore, numerical problems may arise if one wants to apply the same parameterization algorithm to a marine-, truck-, or a small automotive-size compressor, since mass flow and compressor speed values are very dependent of the compressor size.

Both submodels are introduced in the following sections. First an overview is given for the compressor mass flow, and after that the efficiency submodel is thoroughly motivated. To sum up, 21 parameters are required to define the proposed model, 15 for the mass flow submodel and 6 more for the efficiency submodel.

### Mass Flow Model

The Ellipse model, originally developed and motivated in [28, 29], is used to define the mathematical relation between the mass flow and the pressure ratio. Note that the Ellipse model is invertible, so if a surge simulation is required, it can be inverted to compute pressure ratio given mass flow and compressor speed and thus agreeing to the modeling framework proposed by [30]. A sketch of the model and its main characteristics is presented in Figure 3. Furthermore, it is worth mentioning that the model is capable to extrapolate outside the map measured area, and even extrapolate to pressure ratios below unity. Detailed information about the extrapolation capability is omitted in this paper but can be found in [29].

For mass flows greater than ZS flow and smaller than the choke flow ( $\bar{W}_{ZS} \leq \bar{W}_c < \bar{W}_{Ch}$ ) the mass flow pressure ratio relation is given by the implicit function form of an ellipse

$$\left( \frac{\bar{W}_c - \bar{W}_{ZS}}{\bar{W}_{Ch} - \bar{W}_{ZS}} \right)^{CUR} + \left( \frac{\Pi_c - \Pi_{Ch}}{\Pi_{ZS} - \Pi_{Ch}} \right)^{CUR} = 1 \quad (8)$$

where  $\bar{W}_{Ch}$ ,  $\Pi_{Ch}$ ,  $\bar{W}_{ZS}$ ,  $\Pi_{ZS}$  and  $CUR$  are base parameters defined with functions of compressor speed. The base functions are normalized either with the maximum measured mass flow  $\bar{W}_{c,max}$ , or the maximum measured pressure ratio  $\Pi_{c,max}$ . The compressor speed used inside the base functions is also normalized with the maximum compressor speed measured in the map

$$\bar{N}_{c,n} = \bar{N}_c / \bar{N}_{c,max} \quad (9)$$

Originally the choking mass flow base function, described and motivated in [29], was defined by a piecewise function consisting of two equations. This piecewise function was motivated because the measurements show a switching behavior in the increase rate of the choking mass flow as function of compressor speed. This switching characteristic, as described in [29], is normally found around 80% of the maximum compressor speed. A slight modification is proposed here in order to agree with the observed behavior but at the same time avoid the discontinuity introduced by the piecewise function in the derivative of the

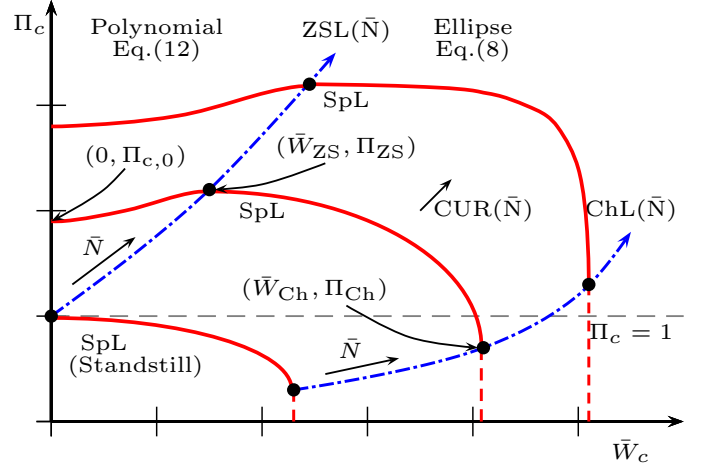


Figure 3: Sketch of the main characteristics of the Ellipse model. The speed lines (SpL) are drawn in solid red, with its vertical extension in the choked area as dashed red line. The choking and zero slope lines are plotted in dashed-dotted blue lines. The dashed gray line situates where the pressure ratio equal to unity is. Note that the curvature increases with speed, and the lowest SpL corresponds to standstill.

choking mass flow. Since having a continuous model is valuable specially when it is used for simulation. Thus, the choking mass flow  $\bar{W}_{Ch}$  base function is defined with the help of an arctan function as follows

$$\bar{W}_{Ch}(\bar{N}_{c,n}) = \bar{W}_{c,max} (c_1 + c_2 \arctan(c_3 \bar{N}_{c,n} - c_4)) \quad (10)$$

where  $c_{1-4}$  are parameters to be estimated.

The rest of the base parameters ( $\Pi_{Ch}$ ,  $\bar{W}_{ZS}$ ,  $\Pi_{ZS}$ ,  $CUR$ ) have the following definitions

$$\Pi_{Ch}(\bar{N}_{c,n}) = \Pi_{c,max} (c_5 + c_6 \bar{N}_{c,n}^{c_7}) \quad (11a)$$

$$\bar{W}_{ZS}(\bar{N}_{c,n}) = \bar{W}_{c,max} (c_8 \bar{N}_{c,n}^{c_9}) \quad (11b)$$

$$\Pi_{ZS}(\bar{N}_{c,n}) = 1 + (\Pi_{c,max} - 1) c_{10} \bar{N}_{c,n}^{c_{11}} \quad (11c)$$

$$CUR(\bar{N}_{c,n}) = c_{12} + c_{13} \bar{N}_{c,n}^{c_{14}} \quad (11d)$$

where  $c_{5-14}$  are parameters to be estimated.

The surge line and the ZS line are not coincident. However, these two lines are not far away, and in particular they are quite close at low compressor speeds, see [28]. This unstable arc, for mass flows smaller than ZS flow ( $\bar{W}_c < \bar{W}_{ZS}$ ), is modeled using the third-order polynomial proposed in [28]

$$\Pi_c = \Pi_{c,0} + 3 \frac{\Pi_{ZS} - \Pi_{c,0}}{\bar{W}_{ZS}^2} \bar{W}_{el}^2 - 2 \frac{\Pi_{ZS} - \Pi_{c,0}}{\bar{W}_{ZS}^3} \bar{W}_{el}^3 \quad (12)$$

where  $\bar{W}_{el}$  is an artificial mass flow, introduced here to allow the model to adapt better to the measured data.  $\bar{W}_{el}$  is defined by the following ellipse function

$$\bar{W}_{el} = \bar{W}_{ZS} \left( 1 - \left( 1 - \frac{\bar{W}_c}{\bar{W}_{ZS}} \right)^{c_{15}} \right)^{1/c_{15}} \quad (13)$$

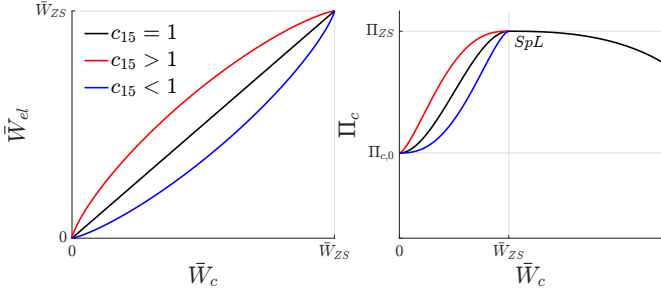


Figure 4: Sketch of the shape of the unstable arc depending on the parameter  $c_{15}$ . Left plot corresponds to the shape of equation (13). Right plot shows for the same  $c_{15}$  values, the shape change in equation (12).

where  $c_{15}$  is an estimation parameter that shapes the third-order polynomial in (12). When  $c_{15} = 1$ , the artificial mass flow is equal to the corrected compressor mass flow  $\bar{W}_{el} = \bar{W}_c$ , and thus (12) is not modified. If  $c_{15} < 1$ , the artificial mass flow lags behind the true compressor mass flow, and the SpL curve (12) moves to the right. On the other hand, when  $c_{15} > 1$ , the artificial mass flow advances the true compressor mass flow and thus the SpL curve (12) moves to the left. A sketch of the flexibility introduced in the model by (13) can be seen in Figure 4.

The pressure ratio at zero flow  $\Pi_{c,0}$  is defined as

$$\Pi_{c,0} = \Pi_{ZS} - \Gamma_{\Pi_{cs}}(\Pi_{ZS} - 1) \quad (14)$$

where  $\Gamma_{\Pi_{cs}}$  is a constant that can be adjusted for a given map if surge measurements are available. Since this is not normally the case in the standard compressor maps, the value is fixed here to  $\Gamma_{\Pi_{cs}} = 1/2$ , following the rules of thumb from [31]. Furthermore, the model can be extended for reverse flows using a turbine mass flow model, see [19], since in this region the compressor can be seen as a poorly designed turbine.

For mass flows greater than the choke flow ( $\bar{W}_c > \bar{W}_{Ch}$ ) the model is assumed to be a vertical line. This is done to resemble the choking physical meaning. So for any pressure ratio smaller than the choking pressure ratio  $\Pi_{Ch}$ , the compressor mass flow is saturated at  $\bar{W}_{Ch}$ . In case this saturation is not suitable for the simulation model, it can be extended in this region with the equation proposed in [29], however this extension is not further investigated here.

## Efficiency Model

The efficiency model presented here is an extension of the model presented in [15], but focused on vaneless automotive radial compressors. Moreover, the main goal in the efficiency modeling is to have a model capable of predicting the efficiency at low compressor speeds for a given compressor map with adiabatic efficiency measurements. As pointed out in Section 2, heat transfer greatly influences the efficiency measurements accuracy, specially at low SpLs. As shown in [10], the maximum

adiabatic efficiency per SpL is quite constant, so the drop in efficiency when speed decreases observed in most manufacturer maps is a direct consequence of the heat transfer. Thus, the model has to be able to keep a high maximum efficiency, per SpL, at low compressor speeds.

The novel idea in the development of the model is to relate the previous linear modeling in the  $\Delta h_{act} - W_c$  plane, see e.g. in [6, 32], to a more general model which incorporates the investigations from [27, 23] for the shape of the SpLs in the  $\lambda - \phi_1$  plane. The derivation of the base functions for the efficiency model starts with equation (5). Using the definitions of the work input and flow coefficients from [18]

$$\lambda_{Euler} = \frac{\Delta h'_{act}}{U_2^2} \quad \phi_1 = \frac{W_c}{\rho_{01} D_2^2 U_2} \quad (15)$$

the equation (5) can be written in the  $\Delta h'_{act} - W_c$  plane as

$$\Delta h'_{act} = \left(1 - \frac{c_s}{U_2}\right) U_2^2 + W_c \frac{U_2}{\rho_{01} D_2 b_2 \pi} \frac{\tan \beta_2}{[1 + (\gamma - 1) \gamma_{imp} \lambda M_{U_2}^2]^{\frac{1}{n_{imp} - 1}}} \quad (16)$$

where  $\Delta h'_{act}$  is used instead of  $\Delta h_{act}$  to distinguish between the actual enthalpy computed with or without the disc friction losses defined by (6). In [15] the actual enthalpy was modeled as an affine function of mass flow. With the affine function parameters depending only on compressor speed with the following structure

$$\Delta h'_{act} = b(U_2) - a(U_2) \cdot W_c \quad (17)$$

identifying the terms  $b$  and  $a$  in (16) yields

$$b(U_2) = \left(1 - \frac{c_s}{U_2}\right) U_2^2 \quad (18a)$$

$$a(U_2) = \frac{U_2}{\rho_{01} D_2 b_2 \pi} \frac{\tan \beta_2}{[1 + (\gamma - 1) \gamma_{imp} \lambda M_{U_2}^2]^{\frac{1}{n_{imp} - 1}}} \quad (18b)$$

It is important to mention that the theoretical expression, (15), is not defined with the corrected quantities of mass flow and compressor speed introduced in (1) and (2). However, in the following definition and motivation of the base functions for the efficiency model, the corrected quantities are used. This is done because in the majority of the conventional compressor maps the only signals available are the corrected quantities. Furthermore, this is shown to give good modeling results later in Section 6 and it gives a convenient way to include variations in the different inlet conditions in the model. Note also that for the majority of the maps, the corrected quantities are equal to the uncorrected quantities since  $T_{01} = T_{c,ref}$  and  $p_{01} = p_{c,ref}$ .

Looking at (18a), and assuming that the slip factor  $c_s/U_2$  remains roughly constant along a speed line,  $b$  should be a quadratic function of compressor speed. In [15, 32] it was taken as a quadratic polynomial of compressor speed with a linear term to increase the model capability to fit a given compressor map data. Having a linear term implies that when transforming the base functions from the  $\Delta h_{act} - W_c$  plane to the  $\lambda_{Euler} - \phi_1$

plane dividing by  $U_2^2$ , the linear term will correspond to a term depending on the inverse of compressor speed. If the magnitude of the estimated linear parameter is not too small, the inverse term will make the  $\lambda_{Euler} - \phi_1$  lines vertical when the compressor speed tends to zero. This is of course not desirable because it does not agree with the results reported in [27]. In order to still have some model flexibility, what is proposed here is a third order polynomial of compressor speed without the linear term, which will correspond to a linear compressor speed variability in the  $\lambda_{Euler} - \phi_1$  plane. The base function, normalized with the maximum measured actual enthalpy rise  $\Delta h_{act,max}$  is defined as

$$b(\bar{N}_{c,n}) = \Delta h_{act,max}(c_{16} \cdot \bar{N}_{c,n}^2 + c_{17} \cdot \bar{N}_{c,n}^3) \quad (19)$$

where  $c_{16}$  and  $c_{17}$  are parameters to be estimated for a particular compressor map.

The slope in the affine function can be identified to (18b). Defining a base function of compressor speed is more complex because many more parameters come into play to represent the change in density at the impeller stage. In [15] the  $a$  base function was rather simplified assuming that the density would remain constant. Here the base function is selected to obtain a more accurate model, which takes into consideration the density change. Observing (18b), it can be seen that it depends linearly on compressor speed due to the numerator  $U_2$  term. A speed dependence is also observed through the tip-speed Mach number present in the denominator. The proposed base function, keeps the structure of (18b) to capture as much as possible the physics of the density change equation. Its normalized mathematical expression is as follows

$$a(\bar{N}_{c,n}) = \frac{\Delta h_{act,max}}{\bar{W}_{c,max}} \frac{c_{18} \bar{N}_{c,n}}{[1 + c_{19} \bar{N}_{c,n}^2]^{c_{20}}} \quad (20)$$

where  $c_{18-20}$  are parameters to be estimated. Ideally  $c_{20}$  should not be a constant, so that it is able to capture changes in  $\gamma_{imp}$  and  $\lambda$  for different speeds and mass flows. However, it is chosen to be a constant to keep the model complexity low and to avoid overfitting.

Finally, the last parameter of the efficiency model is used to account for the nonlinearity of the SpL at low flows. Introducing this parameter will improve the model accuracy, at a price of losing the linearity of the previous model approach. This nonlinearity is mainly due to disk friction but other losses like leakage and recirculation are contributing to it, see e.g. [33]. This can be seen in Figure 1, where the Euler work input coefficient still bends upwards at low flows. The mathematical expression is derived by rewriting (6) as

$$\Delta h_{act} = \left(1 + \frac{c_{21} \rho_{01} D_2^3 \pi \bar{N}_c}{60 \bar{W}_c}\right) (b(\bar{N}_{c,n}) - a(\bar{N}_{c,n}) \bar{W}_c) \quad (21)$$

where  $c_{21}$  is the last parameter of the model. Note that the constants,  $\rho_{01}$ ,  $D_2^3$  and  $\pi$  could be lumped inside the estimation parameter  $c_{21}$ . However keeping them in the expression makes the estimation parameter normalized to the compressor size. In case those parameters are not available in the map, values for

any other similar size compressor will also be suitable, since the estimation parameter will be adjusted to the given compressor map during the parameterization.

## 5 MODEL PARAMETERIZATION

With the compressor model described in Section 4, the following task is to design an algorithm that parameterizes the model to achieve a good fit to a given compressor map. As it is pointed out in [34], the parameterization of compressor models is not trivial because of the asymptotic behavior of the compressor map close to the surge and choke areas as well as the high nonlinearities of the proposed model. A tailored least-squares algorithm is described in this section to be able to provide good parameters for any automotive compressor map. MATLAB is used to implement the parameterization algorithm, with `lsqnonlin` used as the least-squares solver.

### Parameter Initialization

When solving nonlinear least-squares problems, having good initialization values for all the parameters is crucial to obtain good results. In order to find a set of initialization values for any compressor, a separated least-squares problem for each SpL of each compressor map available in the database is solved. This is done in a very similar way in [28] for the  $\bar{W}_{ZSL}$  and  $\Pi_{ZSL}$  base functions, here it is extended for the rest of the model parameters. For the efficiency base functions, only the heat corrected maps are used, this is done to have initialization parameters that set the shape of the modeled efficiency as close as possible to the adiabatic efficiency for a given map.

The results of the separated least-squares problems are used to initialize the parameters of the base functions (equations (10), (11), (19) and (20)), since those depend of compressor speed. Moreover, results from the complete model parameterization are also included to reduce the influence of outliers. A single least-squares problem is then solved for each base function to find the initialization parameters. The results together with the initial parameters,  $k_{num}$ , at the top left corner can be seen in Figures 5, 6, 7, 8, 9, 10 and 11. Since the model equations are normalized, the initialization parameters  $k_{num}$ , can be used directly as  $c_{num}$ , to initialize any compressor model.

A value of  $k_{15} = 1$ , is suitable as initial guess for the parameter  $c_{15}$ . To initialize  $c_{21}$ , the mean value from the estimation of the heat corrected maps is taken. This yields the following initialization value;  $k_{21} = 0.0111$ , which is larger than the usual values given to the parameter when it only represents disk friction, see [27].

### Mass Flow Model Parameterization

The usefulness of minimizing the orthogonal distance between the modeled SpLs and the measured points is highlighted in [15]. This approach avoids parameterization problems when the model becomes vertical near the choking line, or near the ZSL if

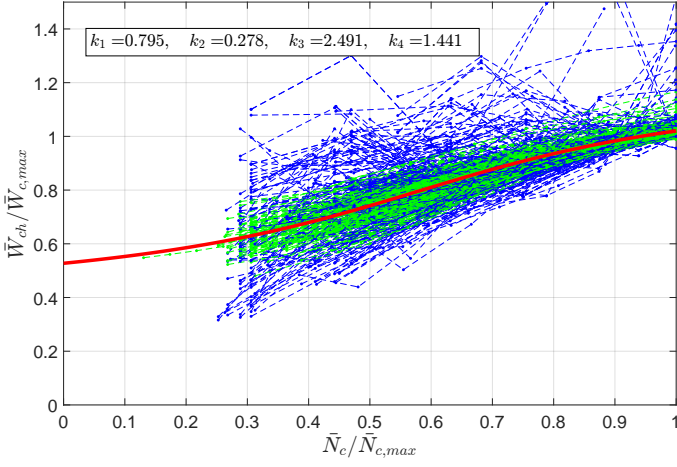


Figure 5: Choke mass flow initialization. Values of the separated SpL estimation are plotted in blue dots with connecting dashed lines for the same compressor. Results from the total model parameterization are depicted in green. Least squares fit is shown in thick red line with the fitted parameters at the top left corner.

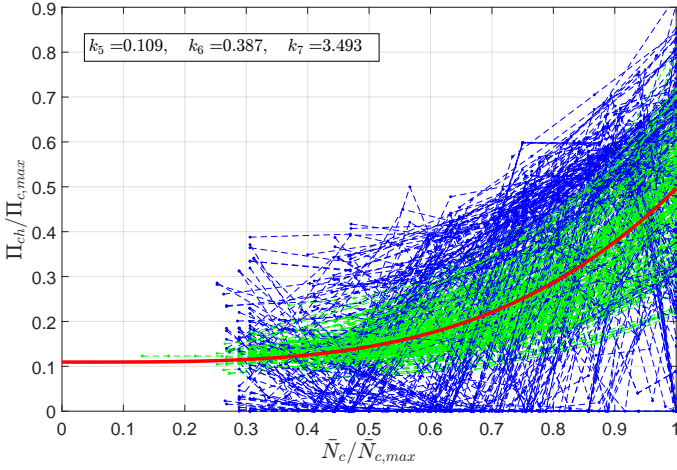


Figure 6: Choke pressure ratio initialization. Values of the separated SpL estimation are plotted in blue dots with connecting dashed lines for the same compressor. Results from the total model parameterization are depicted in green. Least squares fit is shown in thick red line with the fitted parameters at the top left corner.

the model is inverted. This idea is not abandoned here, instead, a novel approach to compute the orthogonal distance based in Total Least-Squares (TLS) is introduced. The main reason for this new approach is because, with TLS, the algorithm becomes computationally quicker and thus it is better suited to deal with the estimation of a large number of compressor maps available in the studied database.

The main characteristic of TLS is that it allows deviations ( $\delta$ ) in the independent variable, in this case corrected mass flow

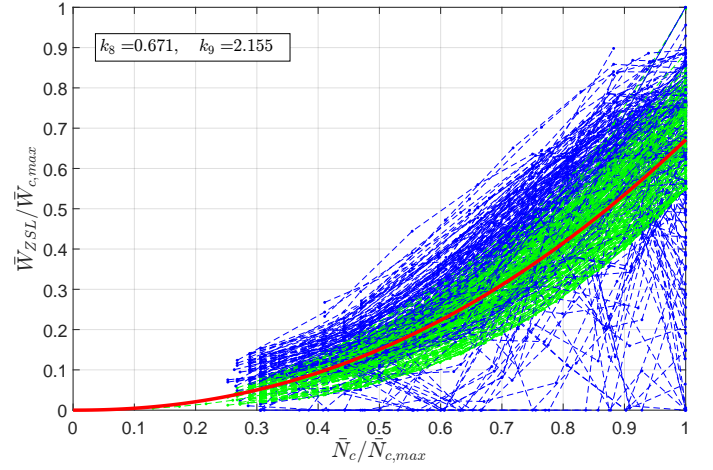


Figure 7: ZSL mass flow initialization. Values of the separated SpL estimation are plotted in blue dots with connecting dashed lines for the same compressor. Results from the total model parameterization are depicted in green. Least squares fit is shown in thick red line with the fitted parameters at the top left corner.

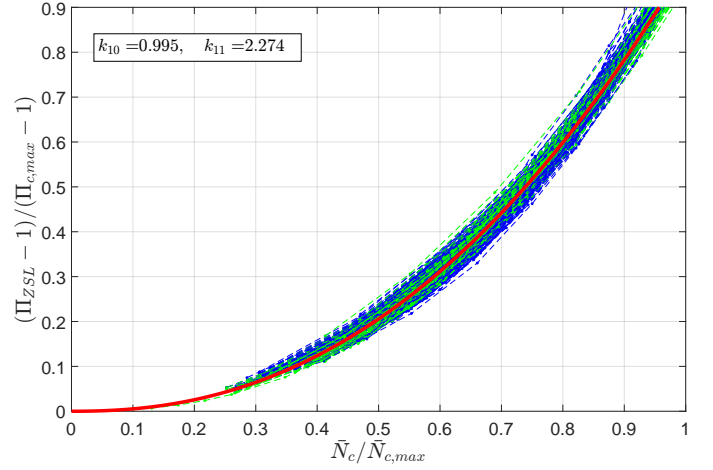


Figure 8: ZSL pressure ratio initialization. Values of the separated SpL estimation are plotted in blue dots with connecting dashed lines for the same initialization. Results from the total model parameterization are depicted in green. Least squares fit is shown in thick red line with the fitted parameters at the top left corner.

$\bar{W}_c$ , when computing the residuals for the least-squares problems. The residuals are computed using the errors in the dependent variable  $\epsilon$  as well as the deviations in the independent variable  $\delta$ . If both errors are weighted with the same value, the formulation becomes equivalent to minimizing the orthogonal distance which is the desired result, see [35] for more information about TLS.

For the mass flow model, which involves the first 15 model

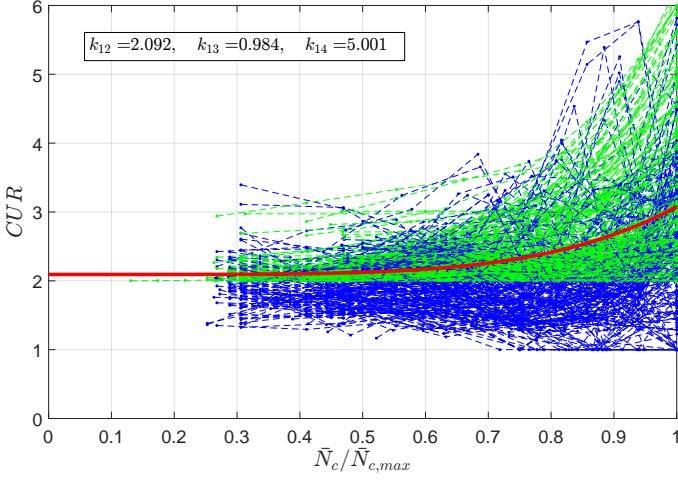


Figure 9: Curvature initialization. Values of the separated SpL estimation are plotted in blue dots with connecting dashed lines for the same compressor. Results from the total model parameterization are depicted in green. Least squares fit is shown in thick red line with the fitted parameters at the top left corner.

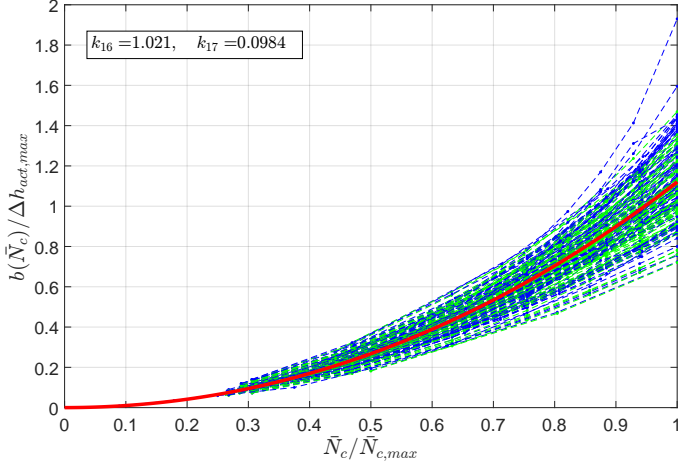


Figure 10: Initialization of base function  $b$ . Values of the separated SpL estimation are plotted in blue dots with connecting dashed lines for the same compressor. Results from the total model parameterization are depicted in green. Least squares fit is shown in thick red line with the fitted parameters at the top left corner.

parameters, the residuals are computed as follows

$$\min_{\theta, \delta} = \sum_{k=1}^m (\epsilon_k^2 + \delta_k^2) \quad (22)$$

with,

$$\epsilon_k = \Pi_{c,k} - f(\theta; \bar{W}_{c,k} + \delta_k), \quad \text{for } k = 1, 2, \dots, m, \quad (23)$$

where  $\theta$  is the vector of the 15 model parameters and  $m$  is the number of measured map points. Note that the  $m$  deviations,  $\delta$ , are treated as estimation parameters in the optimization and thus

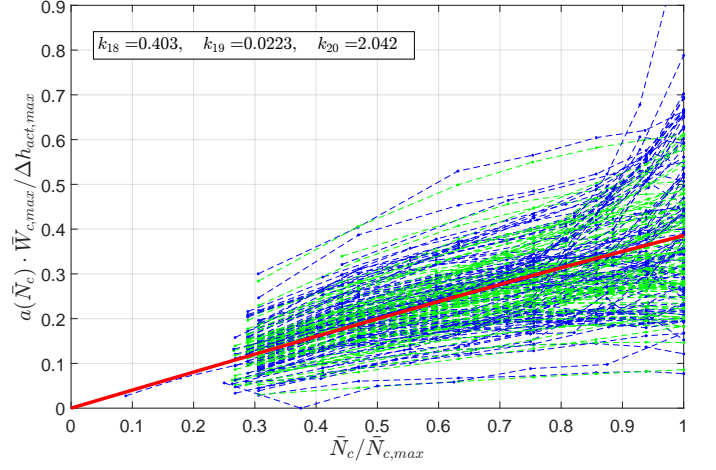


Figure 11: Initialization of base function  $a$ . Values of the separated SpL estimation are plotted in blue dots with connecting dashed lines for the same compressor. Results from the total model parameterization are depicted in green. Least squares fit is shown in thick red line with the fitted parameters at the top left corner.

the estimation problem complexity increases substantially. The piecewise function  $f$  computes the model pressure ratio given mass flow and compressor speed (omitted here for simplicity), with three different areas. For mass flow values greater than the choking mass flow at the current speed, a linear model is used to have a continuous mathematical expression. It is defined by the following equation

$$\Pi_c = \frac{(1 + k_{lin})\Pi_{Ch}}{k_{lin}} - \frac{\Pi_{Ch}}{\bar{W}_{Ch}k_{lin}}\bar{W}_c \quad (24)$$

where  $k_{lin}$  is a parameter that determines the slope of the linear model, ideally infinite to resemble the vertical choke line. Here its value chosen to be 0.01. To sum up,  $f$  is defined, for a given SpL, in the three distinct zones as

$$f(\theta; \bar{W}_c) = \begin{cases} \text{equation (12)} & \bar{W}_c < \bar{W}_{ZSL} \\ \text{equation (8)} & \bar{W}_{ZSL} \leq \bar{W}_c < \bar{W}_{Ch} \\ \text{equation (24)} & \bar{W}_c > \bar{W}_{Ch} \end{cases} \quad (25)$$

Note that (8) is written in implicit form and it needs to be solved for  $\Pi_c$ . Figure 12 contains a sketch of the TLS applied to the mass flow model with the proposed formulation.

### Complete Model Parameterization

The efficiency model proposed in Section 4 requires the compressor mass flow as input to the model. Since mass flow is not available as an external input in a normal MVEM simulation, see (7), it has to be calculated using the mass flow model. This implies that the errors from the mass flow model will affect the efficiency model. Hence, a complete model parameterization to find all compressor parameters at the same time is very important to get a good model accuracy in all three dimensions

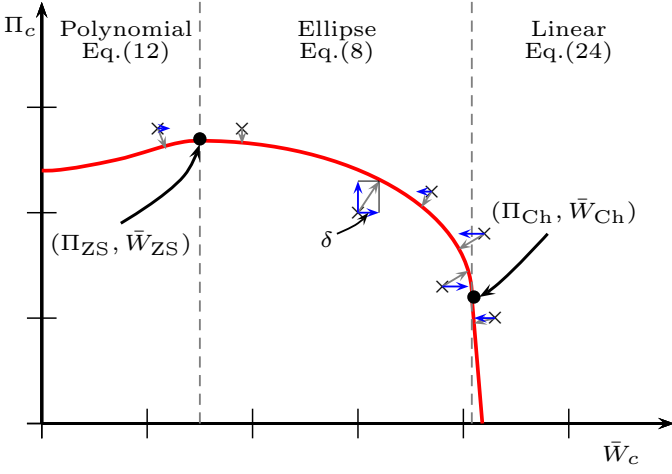


Figure 12: Sketch of the TLS algorithm applied to the model. The modeled curve is seen in solid red, with the three different areas of the  $f$  function. The crosses represent measurement points with the computed distance to the model as gray arrows. The deviations  $\delta$  are represented with blue arrows.

$(\bar{W}_c, \Pi_c, \eta_c)$ , see [15]. This is done as in the previous section by solving a TLS problem to minimize the orthogonal distance in the three dimensions between model and measurements. In order to improve the parameterization, the mass flow parameters obtained estimating the mass flow model alone are used here as initial guess.

The formulation is very similar to the case for the mass flow model alone, the main difference is that it is augmented with the efficiency dimension. The residuals to minimize can be expressed as

$$\min_{\tilde{\theta}, \delta} = \sum_{k=1}^m (\kappa_k^2 + \epsilon_k^2 + \delta_k^2) \quad (26)$$

with,

$$\kappa_k = \eta_{c,k} - g(\tilde{\theta}; \bar{W}_{c,k} + \delta_k, f(\tilde{\theta}; \bar{W}_{c,k} + \delta_k)), \quad (27)$$

$$\epsilon_k = \Pi_{c,k} - f(\tilde{\theta}; \bar{W}_{c,k} + \delta_k), \quad (28)$$

for  $k = 1, 2, \dots, m$ ,

where  $\tilde{\theta}$  is the total vector of model parameters, 21 in total. The function  $g$  computes the compressor efficiency from mass flow and pressure ratio ( $\bar{N}_c$  is again omitted for simplicity). Using equation (21) and the isentropic efficiency definition it can be written as

$$g(\tilde{\theta}; \bar{W}_c, \Pi_c) = \frac{c_p T_{01} \left[ \Pi_c^{\frac{\gamma_c - 1}{\gamma_c}} - 1 \right]}{\Delta h_{act}} \quad (29)$$

## 6 MODEL VALIDATION

The model is parameterized for each of the 234 compressor maps available in the database introduced in Section 3. The ab-

Table 1 Absolute relative errors (%) of the model vs the measurements for the complete database of compressor maps. Mean indicates the mean value of the selected maps in the column while Max. is the maximum value for the maps in that column.

	All Maps		H. corrected		H. uncorrected	
	Mean	Max.	Mean	Max	Mean	Max
$\bar{W}_c$	0.77	2.27	0.72	1.34	0.79	1.61
$\Pi_c$	0.76	1.53	0.71	1.40	0.75	1.36
$\eta_c$	0.83	2.18	0.78	1.78	0.85	2.10

solute relative error of the model for a given signal is computed as

$$e_{rel,j} = \frac{|X_{model,j} - X_{meas,j}|}{\text{mean}(X_{meas})} \cdot 100 \quad (30)$$

where  $X$  can be either  $(\bar{W}_c, \Pi_c, \eta_c)$ , and  $j$  indicates a single measurement index. For a single map, the mean value of the absolute relative error of all measured points is computed. These values are used to compute the mean for the complete database, which is presented for each dimension in the first column of Table 1. This table also contains the maximum mean value of all maps, this is done to benchmark the worst case in each dimension  $(\bar{W}_c, \Pi_c, \eta_c)$ . The errors are below 1% in all three dimensions showing the good model agreement. Furthermore, the model presents similar error values in all three dimensions, which indicates that the complete parameterization introduced in Section 5 balances well the model.

For the maps with available impeller diameter  $D_2$ , the results of the model parameterization with and without the heat transfer correction are available also in Table 1. The errors are below 0.85% in each dimension for the uncorrected case, in particular the fit is better, below 0.78%, when the heat transfer is corrected. This is however not a conclusive result since the heat correction method introduces uncertainty as discussed previously and cannot guarantee the true adiabatic efficiency for a given compressor map. Nevertheless it is a good result to see that the model is very flexible, since it can cope with the heat corrected maps which have higher efficiency values at the lower speeds, and at the same time it adapts with a similar accuracy to the uncorrected maps.

### Heat Corrected Maps

A compressor map is selected out of the 98 compressor maps with available  $D_2$  measurement for a more in-depth analysis of the parameterization results. The parameterized mass flow model, with and without heat correction is depicted against the measurements in Figure 13. The mass flow and pressure measurements are not affected by the heat correction, however the models have small differences as it can be seen in Figure 13. The reason for this is that the complete parameterization is affecting the complete model, it has to slightly adjust the mass flow parameters in order to balance the complete model, also in

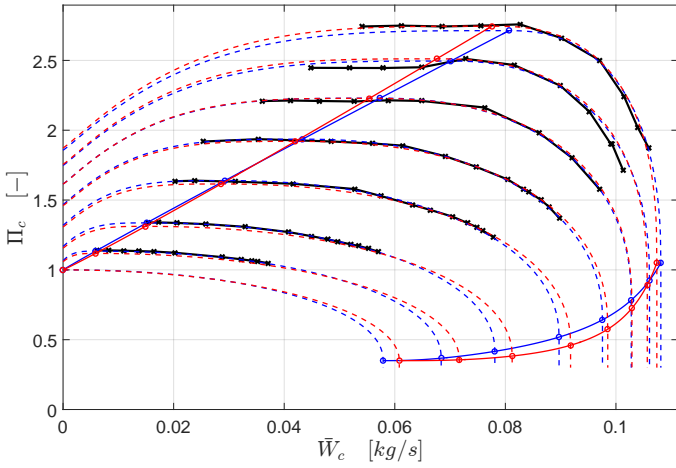


Figure 13: Compressor mass flow vs pressure ratio. The black lines connect the measurement points, the red lines the model parameterized without heat correction, the blue lines correspond to the model with heat correction applied to the data.

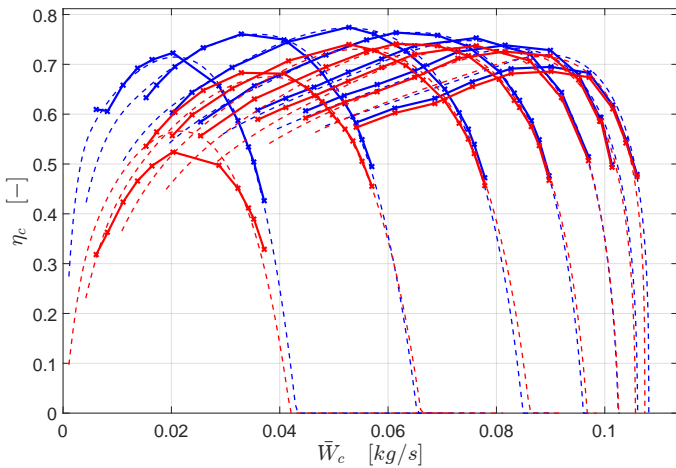


Figure 14: Compressor efficiency vs mass flow. The red lines correspond to the model, dashed, and the measurements, solid, without heat transfer correction. The blue lines correspond to the same description but with heat correction applied to the compressor map.

the efficiency direction.

If the heat correction effects are compared in the efficiency model, the results have a larger impact. Figure 14 contains model vs measurements for the same compressor with and without heat correction. As can be observed, the model is capable to describe well the efficiency with and without the heat transfer correction, which indicates that the model is flexible enough to adapt to any compressor map. The errors are in general low, as can be seen in Table 2, but slightly better if a heat corrected map is used, which is in agreement with the results for all compressor maps shown in Table 1.

For this particular compressor map, the differences in the

Table 2 Absolute relative errors (%) of the model vs the measurements for the compressor map with and without heat transfer correction and for the TD04 and K04 maps. Mean indicates the mean value of the absolute relative error while Max. is the maximum relative error computed.

	H. corrected		H. uncorrected		TD04		K04	
	Mean	Max.	Mean	Max	Mean	Max	Mean	Max
$\bar{W}_c$	0.66	2.35	1.38	5.94	1.74	14.25	0.81	5.90
$\Pi_c$	0.64	2.83	1.00	3.74	0.61	6.78	0.74	3.47
$\eta_c$	0.69	3.69	1.16	4.56	0.79	3.16	0.73	3.37

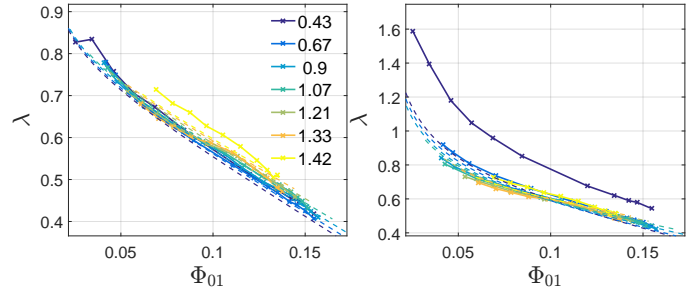


Figure 15: Work input coefficient plotted against mass flow coefficient. Left; with heat correction. Right; no heat correction. The solid lines correspond to measured SpLs, while the dashed lines represent the modeled SpL. The legend values correspond to tip speed Mach number.

$\lambda - \phi_1$  plane with and without heat correction are plotted in Figure 15. It is interesting to see, that the work input coefficient increases with the Mach number as explained in [27], and the modeled SpLs can also describe this increase. To have this dependence, the cubic parameter introduced in (19) is very important, otherwise it would still be possible but it would have had to rely only in the slope parameter  $a$  to resemble this behavior. On the other hand, in the right plot of Figure 15, the agreement is not as good, this is mainly because the model is not capable to represent the SpL with the lowest Mach number which has much larger values than the rest. Note also that with the constant heat correction method from [23], it is not always possible to correct the SpL so that they agree with the increase in work input coefficient as the Mach number increases. This is found to be due to the simplicity of the method as well as because with the little information about the measurement conditions given in the standard used maps, the correction method is difficult to tune properly. An example of this tuning difficulty can be seen in the left plot of Figure 15 where for the lowest SpL, the work input coefficient at the lowest flow coefficient bends downwards. This indicates that the tuning constant could be reduced to avoid it but at the same time all SpL would be affected.

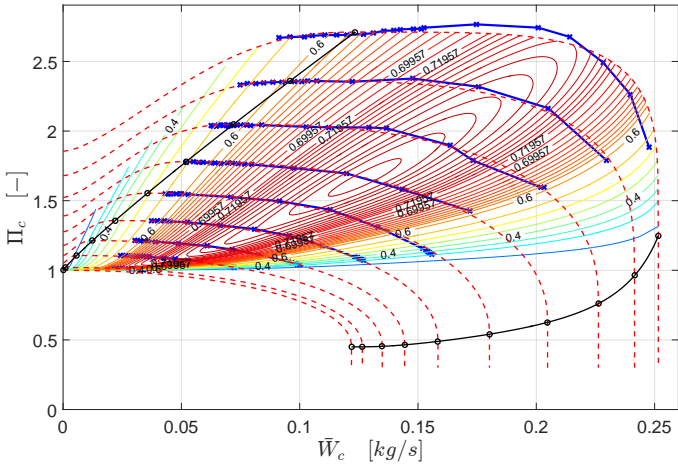


Figure 16: TD04 compressor pressure ratio vs. mass flow. The dashed red lines are the modeled SpLs, the solid blue lines connect the measured points. The contour lines are generated with the efficiency model.

### Low Speed Efficiency Extrapolation

In this section, the capability of the model to extrapolate to low speed values is investigated. This is done by parameterizing the model to two available maps measured with almost adiabatic conditions, see Section 3. These two maps, the TD04 and the K04, contain measurements under the 30% of the maximum compressor speed. The parameterization is done with and without using measured points under the 30% of the maximum compressor speed. This way one can assess how well the model extrapolates under 30% of the compressor speed when it is parameterized with near adiabatic maps. This value of 30% is selected to resemble the lowest SpL available in standard maps, as can be seen in Figure 2.

The good agreement between the model and measurements in the mass flow pressure ratio plane for both compressors can be seen in Figures 16 and 17. Moreover, the model errors, contained in Table 2 are small, with the exception of the mass flow for the TD04 map which is higher than the rest. The results in the efficiency dimension for both compressor maps with and without using the lowest SpLs in the estimation are depicted in Figures 18 and 19. The modeled efficiency is able to keep high values even if the compressor speed drops below the 30% as would be expected in a compressor measured without heat transfer effects. If the SpLs below 30% are used in the estimation, the model fit will improve as it would be expected, since during the parameterization the model gets weighted at this low speed region.

To further assess the extrapolation, the maximum measured efficiency in each speed line is plotted against normalized compressor speed for both compressor maps in Figure 20. The maximum efficiency is quite flat as function of compressor speed, and the model manages to capture this behavior. If the SpLs below 30% are not used, the efficiency still stays at values higher than 60% for speeds higher than 10%. However, when using all

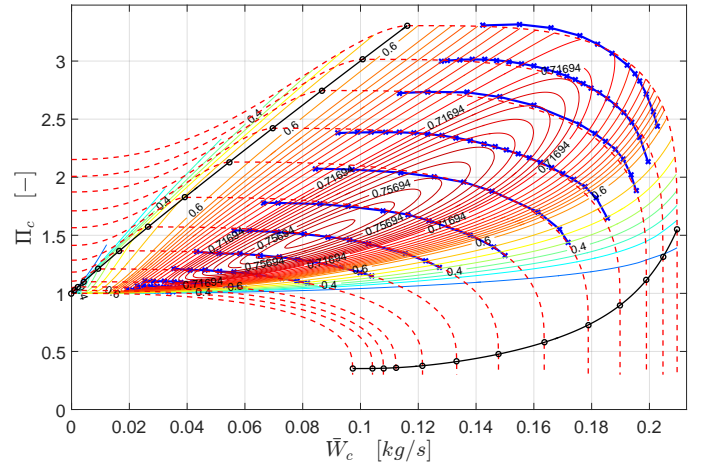


Figure 17: K04 compressor pressure ratio vs. mass flow. The dashed red lines are the modeled SpLs, the solid blue lines connect the measured points. The contour lines are generated with the efficiency model.

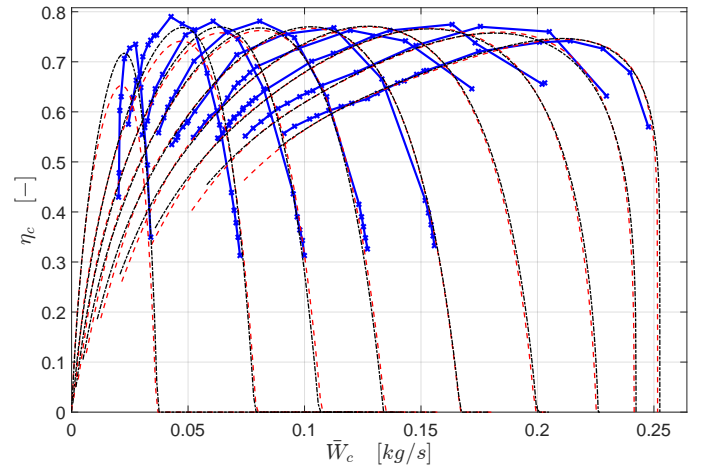


Figure 18: TD04 compressor efficiency vs. mass flow. The solid blue lines connect the measured points, the dashed red lines are the modeled SpLs without using the lowest SpL in the parameterization and the dashed dotted black lines are the modeled SpLs using all available data in the parameterization.

the available data, the model can match the high maximum efficiency values at the lowest SpL much better. It is important to point out that the measured efficiency at SpLs below 30% is difficult to know whether or not is free of measurement errors. This is mainly because the temperature differences used to compute the efficiency are very small and the measurement equipment accuracy can have a big impact in the calculated value, see [14]. As it can be seen in Figures 18 and 19, the measured efficiency has peaks and looks a bit erratic at the lower SpLs, in particular the two lowest SpLs for both maps. This may indicate that some measurement errors may be present. For example, the reason for the higher errors in the mass flow direction for the TD04 map

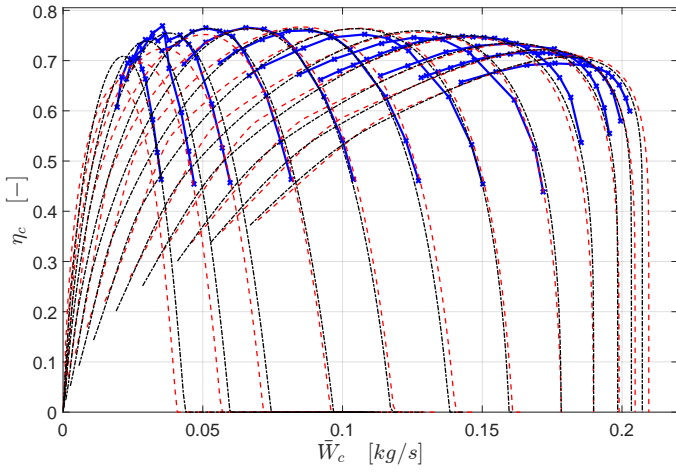


Figure 19: K04 compressor efficiency vs. mass flow. The solid blue lines connect the measured points, the dashed red lines are the modeled SpLs without using the lowest SpL in the parameterization and the dashed dotted black lines are the modeled SpLs using all available data in the parameterization.

can be seen in Figure 18, where for the lowest SpL the measured efficiency drops much faster than the modeled even if the maximum efficiency value is similar. This makes the distance in the mass flow direction between the modeled and measured SpLs large. Nevertheless, one has to take into consideration that errors in the prediction of efficiency might occur for speeds below 30% as can be seen in Figure 19. Repetition of the measurements at low speeds for these and other compressors would be useful to further investigate the extrapolation capabilities of the model.

## 7 CONCLUSIONS

A complete control-oriented compressor model is presented and validated using 234 compressor maps of different sizes. In total the model consists of 21 parameters that have to be estimated from measurement data. The proposed model is capable to extrapolate to low compressor speeds and even compressor ratios below unity. In particular, the efficiency model is improved from previous work to increase the model accuracy using more physical insight. A closer look is given at the efficiency extrapolation to low compressor speeds with the known effects that the heat transfer has in the measured compressor efficiency.

A novel parameterization approach based on TLS is also developed. The algorithm does not require more information about the compressor performance than what is normally included in the standard compressor maps. Furthermore, the estimation takes into consideration that the mass flow and efficiency models are connected. Thus the model is parameterized in the three dimensions at once in order to obtain the best possible compressor performance representation. The results show that the parameterization algorithm works well and it is capable to deal with compressor maps of different sizes and characteris-

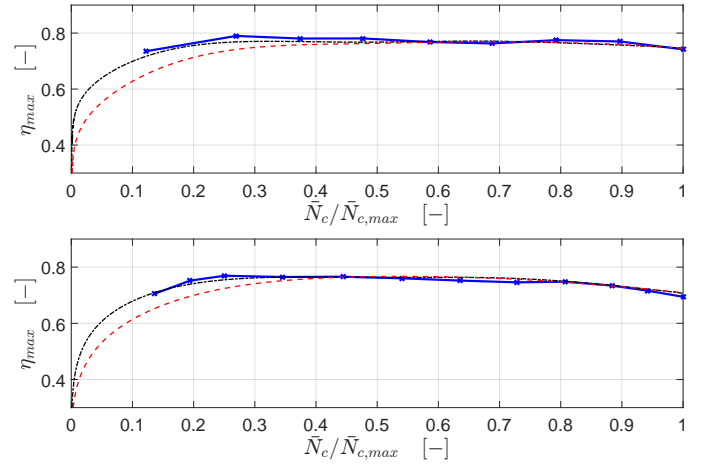


Figure 20: Compressor maximum efficiency vs. normalized compressor speed. Top plot corresponds to the TD04 map and the bottom plot to the K04 map. The solid blue lines connect the measured points, the dashed red lines are the modeled SpLs without using SpLs below 30% in the parameterization and the dashed dotted black lines are the modeled SpLs using all available data in the parameterization.

tics. Furthermore, initialization values for the model parameters are provided in order to avoid problems when trying to estimate a given compressor map.

The model errors in the three dimensions are always below 1% as a mean value. A heat correction method is applied to 98 of the database maps to obtain the adiabatic efficiency. The model is shown to adapt well to the measurement data with and without the heat correction, but in particular the errors are lower when the compressor map has adiabatic efficiency. This indicates that the model can be used with a similar accuracy regardless of how the efficiency is measured. Two maps measured under adiabatic conditions and to lower compressor speeds than usual are used to validate the efficiency extrapolation. The model is shown to be able to keep a flat maximum adiabatic efficiency as function of compressor speed, and to match well the measured values for relative compressor speeds below 30%. If the speeds below 30% are not used in the parameterization, the maximum efficiency accuracy is decreased but still manages to follow the trend to stand still. More measurements in that area for different compressor maps would be very useful to further analyze the model extrapolation characteristics.

## NOMENCLATURE

- ICE** Internal Combustion Engines
- MVEM** Mean Value Engine Model
- SpL** Speed Line
- TLS** Total Least Squares
- ChL* Choke Line
- CUR* Ellipse curvature

$ZSL$  Zero Slope Line  
 $a$  Linear efficiency model slope  
 $b$  Linear efficiency model parameter  
 $b_2$  Diffuser width  
 $c_p$  Specific heat value  
 $c_{num}$  Model parameter  
 $D_2$  Outer impeller compressor diameter  
 $e_{rel}$  Relative error  
 $h_{is}$  Isentropic enthalphy  
 $h_{act}$  Actual enthalphy  
 $k_{num}$  Initialization value  
 $k_{fric}$  Disk friction parameter  
 $M_{U_2}$  Tip-speed Mach number  
 $N$  Rotational speed  
 $\bar{N}$  Corrected rotational speed  
 $n_{imp}$  Polytropic exponent  
 $p$  Pressure  
 $T$  Temperature  
 $U_2$  Blade tip-speed  
 $W$  Mass flow  
 $\bar{W}$  Corrected mass flow

## GREEK SYMBOLS

$\Pi$  Pressure ratio  
 $\gamma$  Isentropic specific heats ratio  
 $\gamma_{imp}$  Kinematic degree of reaction  
 $\epsilon$  Error in pressure ratio  
 $\kappa$  Error in efficiency  
 $\delta$  Deviation in mass flow  
 $\rho$  Density  
 $\eta$  Efficiency  
 $\beta_2$  Outlet blade angle  
 $\phi$  Flow coefficient  
 $\theta$  Vector of parameters  
 $\lambda$  work input coefficient  
 $\Gamma_{\Pi_{cs}}$  Zero flow parameter

## SUBSCRIPTS

01 Inlet total conditions  
 02 Outlet total conditions  
 $c$  Compressor  
 $el$  Ellipse

$n$  Normalized  
 $max$  Maximum  
 $Ch$  Choke  
 $rel$  Relative  
 $ref$  Reference  
 $ZS$  Zero Slope

## CONTACT INFORMATION

Xavier Llamas and Lars Eriksson  
 Vehicular Systems  
 Dept. of Electrical Engineering  
 Linköping University  
 SE-581 83 Linköping, Sweden  
 xavier.llamas.comellas@liu.se  
 lars.eriksson@liu.se

## ACKNOWLEDGMENT



This project has received funding from the European Union's Horizon 2020 research and innovation programme under grant agreement No 634135.

## REFERENCES

- [1] Elbert Hendricks. A compact, comprehensive model of a large turbocharged, two-stroke diesel engine. In *SAE Technical Paper*. SAE, 1986. doi: 10.4271/861190.
- [2] Martin Müller, Elbert Hendricks, and Spencer C. Sorenson. Mean value modelling of turbocharged spark ignition engines. In *SAE Technical Paper 980784*. SAE International, February 1998. doi: 10.4271/980784.
- [3] Merten Jung. *Mean-Value Modelling and Robust Control of the Airpath of a Turbocharged Diesel Engine*. PhD thesis, Sidney Sussex College, Department of Engineering, University of Cambridge, Cambridge, UK, 2003.
- [4] Paul Moraal and Ilya Kolmanovsky. Turbocharger modeling for automotive control applications. In *SAE Technical Paper*. SAE International, March 1999. doi: 10.4271/1999-01-0908.
- [5] Lars Eriksson. Modeling and control of turbocharged SI and DI engines. *Oil & Gas Science and Technology*, 62(4):523–538, October 2007. doi: 10.2516/ogst:2007042.
- [6] Guillaume Martin, Vincent Talon, Pascal Higelin, Alain Charlet, and Christian Caillol. Implementing turbomachinery physics into data map-based turbocharger models. *SAE Int. J. of Engines*, 2(1):211–229, April 2009. doi: 10.4271/2009-01-0310.

- [7] Spencer C. Sorenson, Elbert Hendricks, Sigurjon Magnusson, and Allan Bertelsen. Compact and accurate turbocharger modelling for engine control. In *SAE Technical Paper*. SAE International, 04 2005. doi: 10.4271/2005-01-1942.
- [8] M Taburri, F Chiara, M Canova, and Y-Y Wang. A model-based methodology to predict the compressor behaviour for the simulation of turbocharged engines. *Proc Inst Mech Eng D: Journal of Automobile Engineering*, 226(4): 560–574, 2012. doi: 10.1177/0954407011420790.
- [9] Karla Stricker, Lyle Kocher, Ed Koeberlein, D.G. Van Alstine, and Gregory M. Shaver. Turbocharger map reduction for control-oriented modeling. *ASME J Dyn Sys Meas Control*, 136(4), April 2014. doi: 10.1115/1.4026532.
- [10] Silvia Marelli, Giulio Marmorato, Massimo Capobianco, and Andrea Rinaldi. Heat transfer effects on performance map of a turbocharger compressor for automotive application. In *SAE Technical Paper 2015-01-1287*, 04 2015. doi: 10.4271/2015-01-1287.
- [11] Chesse, P., Chalet, D., and Tauzia, X. Impact of the heat transfer on the performance calculations of automotive turbocharger compressor. *Oil & Gas Science and Technology*, 66(5):791–800, 2011. doi: 10.2516/ogst/2011129.
- [12] Karl D. Wygant Nick Baines and Antonis Dris. The analysis of heat transfer in automotive turbochargers. *ASME J Gas Turb Pwr*, 4(132), January 2010. doi: 10.1115/1.3204586.
- [13] M. Cormerais, J. F. Hetet, P. Chesse, and A. Maiboom. Heat transfer analysis in a turbocharger compressor: Modeling and experiments. In *SAE Technical Paper*. SAE International, 04 2006. doi: 10.4271/2006-01-0023.
- [14] S. Shaaban and J.R. Seume. Analysis of turbocharger non-adiabatic performance. In *8th International Conference on Turbochargers and Turbocharging*, pages 119 – 130. Woodhead Publishing, 2006. doi: 10.1016/B978-1-84569-174-5.50012-9.
- [15] Xavier Llamas and Lars Eriksson. Parameterizing compact and extensible compressor models using orthogonal distance minimization. *ASME J Gas Turb Pwr*, 139(1), 2017. doi: 10.1115/1.4034152.
- [16] SAE J922 – Turbocharger Nomenclature and Terminology. SAE standard, 1995.
- [17] N. Watson and M.S. Janota. *Turbocharging the internal combustion engine*. MacMillan, London, 1982.
- [18] Sydney Lawrence Dixon and Cesare A Hall. *Fluid Mechanics and Thermodynamics of Turbomachinery*. Butterworth-Heinemann, Oxford, UK, 7th edition, 2013. ISBN 9780124159549.
- [19] Lars Eriksson and Lars Nielsen. *Modeling and Control of Engines and Drivelines*. John Wiley & Sons, Hoboken, NJ, 2014.
- [20] Oskar Leufvén and Lars Eriksson. Investigation of compressor correction quantities for automotive applications. *Int. J. Engine Res.*, 13(6):588–606, November 2012.
- [21] Jose Serrano, Pablo Olmeda, Francisco Arnau, Miguel Reyes-Belmonte, and Alain Lefebvre. Importance of heat transfer phenomena in small turbochargers for passenger car applications. *SAE Int. J. Engines*, 6:716–728, 04 2013. doi: 10.4271/2013-01-0576.
- [22] Kristoffer Ekberg and Lars Eriksson. The effect of pressure losses on measured compressor efficiency. In *9th EUROSIM Congress on Modelling and Simulation*, Oulu, Finland, 2016. doi: 10.1109/EUROSIM.2016.169.
- [23] Michael V. Casey and Thomas M. Fesich. The efficiency of turbocharger compressors with diabatic flows. *ASME J Gas Turb Pwr*, 7(132), April 2010.
- [24] Borislav Sirakov and Michael Casey. Evaluation of heat transfer effects on turbocharger performance. In *Proceedings of ASME Turbo Expo*, Vancouver, BC, Canada, June 2011. ASME.
- [25] Michael Casey and Chris Robinson. A method to estimate the performance map of a centrifugal compressor stage. *ASME J Turbomach*, 2(135), 2012. doi: 10.1115/1.4006590.
- [26] Mehdi Nakhjiri, Peter Pelz, Berthold Matyschok, Lorenz Däubler, and Andreas Horn. Apparent and real efficiency of turbochargers under influence of heat flow. In *14th International Symposium on Transport Phenomena and Dynamics of Rotating Machinery (ISROMAC-14)*, Honolulu, HI, February 2012.
- [27] M.V. Casey and M. Schlegel. Estimation of the performance of turbocharger compressors at extremely low pressure ratios. *Proc Inst Mech Eng A: Journal of Power and Energy*, 2(224):239–250, November 2009. doi: 10.1243/09576509JPE810.
- [28] Oskar Leufvén and Lars Eriksson. A surge and choke capable compressor flow model - validation and extrapolation capability. *Control Eng. Pract.*, 21(12):1871–1883, December 2013. doi: 10.1016/j.conengprac.2013.07.005.
- [29] Oskar Leufvén and Lars Eriksson. Measurement, analysis and modeling of centrifugal compressor flow for low pressure ratios. *Int. J. Engine Res.*, 17(2):153–168, February 2016. doi: 10.1177/1468087414562456.
- [30] E. M. Greitzer. The stability of pumping systems - the 1980 Freeman scholar lecture. *Journal of Fluids Engineering*, 103:193–242, 1981.

- [31] Lars Eriksson, Vaheed Nezhadali, and Conny Andersson. Compressor flow extrapolation and library design for the modelica vehicle propulsion library - vehprolib. In *SAE Technical Paper 2016-01-1037*. SAE International, April 2016. doi: 10.4271/2016-01-1037.
- [32] Jamil El Hadeif, Guillaume Colin, Yann Chamaillard, and Vincent Talon. Physical based algorithms for interpolation and extrapolation of turbocharger data maps. *SAE Int. J. of Engines*, 5(2):363–378, April 2012. doi: 10.4271/2012-01-0434.
- [33] Peter Harley, Stephen Spence, Dietmar Filsinger, Michael Dietrich, and Juliana Early. Assessing 1D loss models for the off-design performance prediction of automotive turbocharger compressors. In *Proceedings of ASME Turbo Expo*, San Antonio, Texas, USA, June 2013. ASME. doi: 10.1115/GT2013-94262.
- [34] Daniel Pachner, Lukas Lansky, David Germann, and Markus Eigenmann. Fitting turbocharger maps with multidimensional rational functions. In *SAE Technical Paper 2015-01-1719*. SAE International, April 2015. doi: 10.4271/2015-01-1719.
- [35] Jorge Nocedal and Stephen J. Wright. *Numerical Optimization*. Springer, New York, 2nd edition, 2006.